Nonlinear interferometers for Fourier-transform infrared spectroscopy with visible light

Chiara Lindner, Jachin Kunz, Sebastian Wolf, Jens Kiessling, and Frank Kühnemann

Fraunhofer Institute for Physical Measurement Techniques IPM, Georges-Köhler-Allee 301, 79110 Freiburg, Germany

ABSTRACT

Nonlinear interferometers based on non-degenerate spontaneous parametric down-conversion (SPDC) create a link between separate spectral ranges. This allows for measurements in remote spectral regions while detecting light in easily accessible wavelengths. In our work, we use periodically poled lithium niobate to create correlated signal (visible or near-infrared) and idler (mid-infrared) photon pairs. Using a nonlinear interferometer in Michelson geometry, we obtain broadband mid-infrared spectra from light detected with a silicon avalanche photodiode. Combining the nonlinear interferometer with a measurement scheme in close analogy to classical Fourier-transform infrared spectroscopy allows for sub-wavenumber spectral resolution, which opens up possibilities for applications such as precise spectroscopic gas analysis.

Keywords: Nonlinear Interferometer, Spectroscopy, Quantum optics, Mid-IR, SPDC, Fourier-transform

1. INTRODUCTION

While interference phenomena are often treated in the context of classical wave mechanics, some effects can only be described conclusively using concepts of quantum mechanics. One such example which often requires non-classical treatment is the interference of correlated photon pairs, which are experimentally accessible using spontaneous parametric down-conversion (SPDC). This process can be described as the spontaneous decay of pump photons inside a nonlinear medium. The energy of the pump photon is distributed to two correlated photons of lower energy, called signal and idler. If the photons of one SPDC process are injected into a second SPDC source, second-order interference is observable in both signal and idler intensity due to induced coherence without induced emission.[1] Interestingly, the interference pattern of the signal and idler intensity depends on the transmission and phase of pump, signal and idler between the SPDC sources.[2,3] This effect opens new perspectives for applications and metrology when using non-degenerate SPDC. Using signal and idler photons with a large spectral separation, light detection and sample interaction can be conducted in different spectral regions. Various applications using nonlinear interferometers have been demonstrated, such as optical coherence tomography,[4–6] microscopy,[7,8] sensing[9] and imaging.[10]

Nonlinear interferometers also offer interesting perspectives for mid-infrared spectroscopy.[11–14] This important analytic technique has many applications in industry and science, with well-established powerful techniques such as Fourier-transform infrared spectroscopy (FTIR). Recently developed techniques such as nonlinear optical frequency upconversion spectroscopy[15,16] seek to push beyond the limitation of conventional broadband mid-infrared spectroscopic techniques. Nonlinear interferometers using pairs of correlated mid-infrared and near-infrared photons may offer an alternative measurement approach as they combine mid-infrared photon generation for sample interaction with short-wavelength detection. The silicon-based detectors for the visible or near-infrared spectral range have much lower dark noise and higher bandwidth in comparison to infrared detectors, which in addition often require cooling.

Nonlinear interferometers for infrared spectroscopy analyze the change of the visibility of the signal interference pattern due to the absorption of the correlated idler photons interacting with the sample. Different concepts for retrieving the spectral information have been demonstrated using monochromators or grating-based spectrometers.[11,13] Another approach is to measure the correlation function of the correlated photon pairs and retrieve the spectrum using a Fourier-transform. In a recent publication, Fourier-transform spectroscopy was demonstrated using spatially resolved detection.[14] In this measurement scheme, a series of signal interference patterns was recorded using a silicon-based camera while varying the delay between signal and idler interferometer arm. A

in: Schunemann, P.G.; Schepler, K.L.; Society of Photo-Optical Instrumentation Engineers –SPIE:
SPIE Proceedings Volume 11670, Nonlinear Frequency Generation and Conversion: Materials and Devices XX; 1167010 (2021)
https://doi.org/10.1117/12.2578278

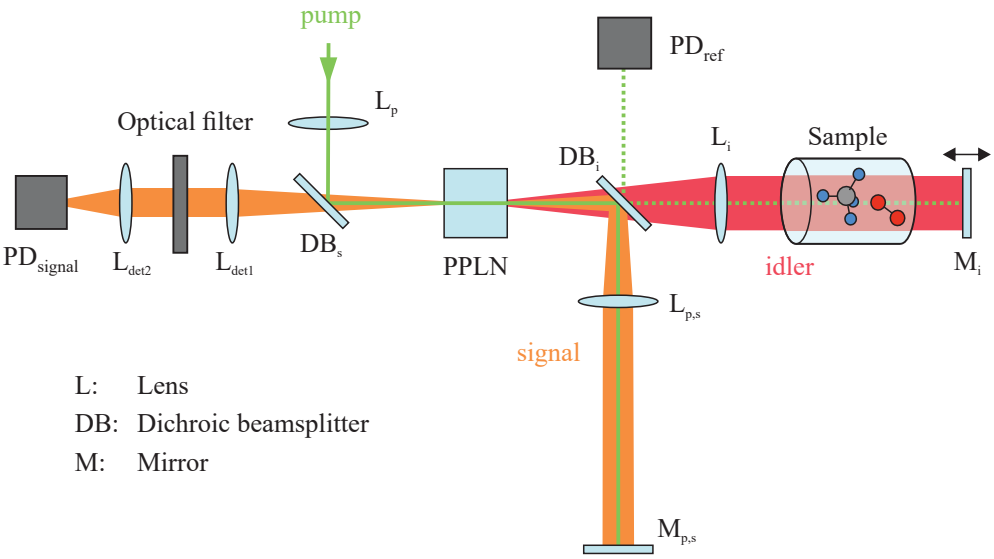

Figure 1. Setup of the nonlinear interferometer

spectral resolution of $6\,\mathrm{cm}^{-1}$ was achieved over an instantaneous bandwidth of $100\,\mathrm{cm}^{-1}$, using non-collinear SPDC emission. Spatially resolved detection using a camera and pixel-wise analysis was required due to a spatially varying phase and optical path difference for the non-collinear components.
In this work we present an approach to Fourier-transform spectroscopy using a nonlinear interferometer with broadband collinear SPDC emission, which allows using a single-pixel near-infrared silicon-based detector. We demonstrate a sub-wavenumber spectral resolution, which is only limited by the maximum interferometer delay. A spectral range of 3.1 µm to 4.0 µm is covered in a single measurement. The spectrometer is characterized using measured transmission spectra of a dilution of methane in nitrogen and a comparison to a simulation based on HITRAN spectroscopic data.

2. EXPERIMENTAL REALIZATION

2.1 Spontaneous parametric down-conversion light source

Key component of the nonlinear interferometer is the spontaneous parametric down-conversion (SPDC) source emitting correlated photons. In general, the sum of signal and idler frequencies equals the pump frequency due to energy conservation. For efficient emission, the three waves inside the nonlinear medium additionally need to be phase matched. In a recent publication,[17] it has been demonstrated that the bandwidth of SPDC can be increased in many nonlinear materials by matching the group indices of signal and idler. In our experiments, we use a 10-mm-long lithium niobate crystal with 5-mol-%-MgO doping and quasi phase matching. In this material, the group velocity at the target center idler wavelength (3.6 µm) is matched with the group velocity around 1 µm wavelength. To achieve phase matching with the resulting pump wavelength (785 nm) a poling period of 21.5 µm and a crystal temperature 65 °C crystal temperature is used. This phase matching configuration allows for an instantaneous near-collinear idler wavelength range of 3.1 µm to 4.0 µm.

2.2 Nonlinear interferometer

The optical set-up of the nonlinear interferometer is shown in Figure 1. The pump laser is a countinuous-wave Ti:sapphire laser with an output power of 700 mW, which is stabilized to 785 nm wavelength with 10 MHz accuracy. The pump laser is focused with lens L_p into the center of the nonlinear crystal (PPLN). The dichroic beamsplitter DB_s reflects the pump beam which passes the nonlinear crystal and causes the SPDC process emitting signal (depicted orange) and idler light (depicted red). The dichroic mirror DB_i separates pump, signal and idler. The mid-infrared idler beam is transmitted by DB_i and collimated using a CaF_2 lens (L_i) with a

focal length of 100 mm. The idler beam passes the sample gas cell, a small cylinder with 20 mm length and anti-reflective coated BaF_2 windows, which can be filled with an analyte or pure nitrogen as reference. The plane gold mirror M_i reflects the idler light, which is imaged back into the nonlinear crystal in an effective $4f$ relay optic. The mirror is mounted on a voice coil translation stage with a maximum displacement of ± 10 mm in beam direction. The pump and signal light, which is is reflected by the dichroic mirror DM_i take an analogue path in the second interferometer arm, which has a fixed $4f$ optical path length.

The back reflected pump beam causes a second SPDC process, which leads to interference of the signal and idler light generated in either pass through the crystal. After the second pass, the pump beam is again reflected by the dichroic beamsplitter DB_s and then removed by an optical isolator. The idler light is absorbed by the dichroic mirror. The signal light carrying the interference pattern is transmitted by the dichroic beamsplitter and collimated by a lens with 100 mm focal length (L_{s2}). Residual pump, idler, and ambient light is removed by an optical 850 nm long pass filter. The signal light is focused onto the active area of the detector PD_{signal}, which is a silicon avalanche photodiode (APD) with a noise equivalent power of $6\,\mathrm{fW}/\sqrt{\mathrm{Hz}}$ and a quantum efficiency of 55.8 %. The detector signal passes an electronic filter with 0.4 kHz to 5 kHz pass band and is digitized with an analog-digital converter.

In order to obtain the spectrum of the interferometer with a Fourier-transform, the interferogram has to be sampled at equidistant positions of the idler mirror M_i. In classical Fourier-transform infrared (FTIR) spectrometers, this is typically achieved by using the sinusodial interferogram of a near-monochromatic laser source with known wavelength as reference.[18] In our set-up, we omit the additional laser and instead take advantage of the residual transmission of the pump beam through the dichroic mirror DM_i (dashed green line in Figure 1). The small portion of pump light (<1%) receives the same retardation as the idler light when the idler mirror M_i is moved. The residual pump beam is then superimposed with the residual transmission of pump light which was originally reflected on the dichroic mirror. The dichroic mirror DM_i and the end mirrors M_i and M_s form a classical Michelson interferometer for the pump beam with a high amplitude contrast between the interferometer arms. The pump beam interference pattern is measured with a photodiode PD_{ref}, the measurement signal passes a high-pass filter and is digitized.

Using a photodiode-based power sensor, a total signal power of (20 ± 1.4) nW was measured, from which we can estimate a corresponding infrared idler power of about 6 nW. The SPDC power depends linearly on the pump power. While the interference *contrast* depends linearly on the transmission of all three beams, the signal *power* is independent on the idler transmission, which verifies that the two SPDC processes are indeed spontaneous and without any stimulated emission. A maximum interference contrast of 15 % is measured as the peak AC/DC ratio of the detector signal (measured without electronic bandpass filter). The interference contrast is limited by dispersion inside the nonlinear crystal, non-ideal reflective and anti-reflective coatings of the optical elements and imperfect beam overlap of the two SPDC processes.

3. MEASUREMENTS AND RESULTS

An interferogram is measured using a nitrogen-filled sample cell for reference, by recording the signal intensity as the idler mirror is moved at a constant velocity of 2 mm/s. The available displacement range of the double-sided interferogram is 18 mm, which corresponds to a theoretical maximum spectral resolution of $0.56\,\mathrm{cm}^{-1}$. The time-referenced interferogram is then transformed into a position-referenced interferogram using the zero-crossing of the pump interference, as described above. In order to increase the signal-to-noise ratio, 100 similar interferograms are recorded and added coherently.

Figure 2(a) shows a section of the resulting normalized interferogram featuring a broad and asymmetric shape, different from typical interferograms observed in a classical FTIR. The irregular shape is caused by the dispersion of the nonlinear crystal, which is inherent to the system and results in a wavelength dependent optical path difference between signal and idler beam throughout the large emission bandwidth. A chirped interferogram yields the same spectral information as an interferogram without dispersion, which has also been demonstrated for classical FTIR spectroscopy.[19]

The position referenced and averaged interferogram is then Fourier-transformed using a discrete Fourier-transform based on the Fast Fourier-transform (FFT) algorithm. The optical power spectral density (PSD) is calculated as the modulus of the complex amplitude of the Fourier-transform. The spectrum of the nonlinear interferometer

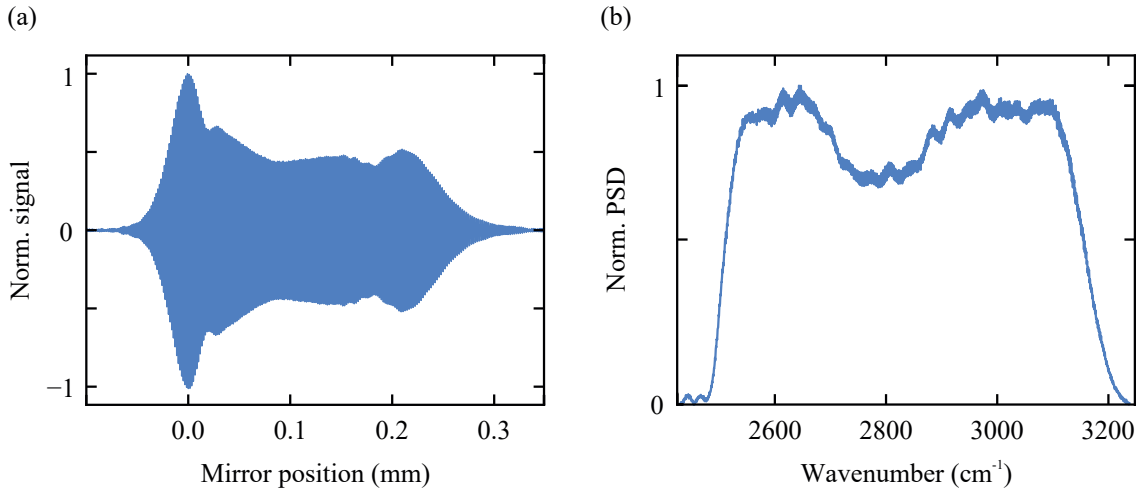

Figure 2. (a) averaged interferogram of 100 reference measurement scans. (b) Normalized power spectral density of the Fourier-transform of the interferogram shown in (a)

(shown in Figure 2(b)) extends over a large bandwidth of over $725\,\mathrm{cm}^{-1}$. The measurement and analysis procedure is then repeated with the sample filled into the gas cell. For a demonstration of a realistic measurement task, we demonstrate measurements of a mixture of 1 % methane in nitrogen at atmospheric pressure.
The transmission of the sample is calculated from the quotient of the power spectral densities of sample and reference spectrum. Using the transmission spectrum shown in Figure 3(a), the performance of the spectrometer can be characterized.

4. SPECTROSCOPIC PERFORMANCE CHARACTERIZATION

4.1 Spectral resolution

The spectral resolution can be characterized by comparing the measured transmission spectrum to an expected transmission spectrum calculated as a convolution of spectroscopic data and an instrument function:

$$T_\mathrm{m}(\tilde{\nu}) = (T_\mathrm{th} * f)(\tilde{\nu}). \tag{1}$$

The spectroscopic data on methane is taken from the HITRAN database,[20,21] using ambient conditions and a Voigt line profile. According to the simulation, the width of individual absorption lines is at the order of $0.12\,\mathrm{cm}^{-1}$ full width at half maximum (FWHM). Main contributor to the width of absorption lines observed in the transmission spectrum is the instrument function $f(\tilde{\nu})$, which can be described by:

$$f(\tilde{\nu}) = \frac{2}{\Delta\tilde{\nu}} \operatorname{sinc}\left(\frac{2\pi\tilde{\nu}}{\Delta\tilde{\nu}}\right). \tag{2}$$

Similar to classical FTIR spectrometers, the spectral resolution $\Delta\tilde{\nu}$ is limited to the maximum interferometer delay, which amounts to $1/L \approx 0.56\,\mathrm{cm}^{-1}$.
The spectral resolution of the measured transmission spectrum can be determined by fitting the expected transmission to the measured data using $\Delta\tilde{\nu}$ as a free parameter. Figure 3 shows the measured transmission spectrum in orange in comparison to the fitted transmission (gray curve). Part b) shows a detailed view of the absorption feature around $3067\,\mathrm{cm}^{-1}$. The fitted transmission spectrum shows good agreement to the measured values and yields a spectral resolution of $0.56\,\mathrm{cm}^{-1}$, which is in agreement to the theoretic value. This shows that the spectral resolution is indeed only limited by the maximum delay between the interferometer arms and can be improved using a setup which allows for larger displacement values. Even in its current realization, the setup achieves a higher spectral resolution than previous implementations of spectrometers based on nonlinear interferometers which rely on gratings for spectral selection.[11,13]

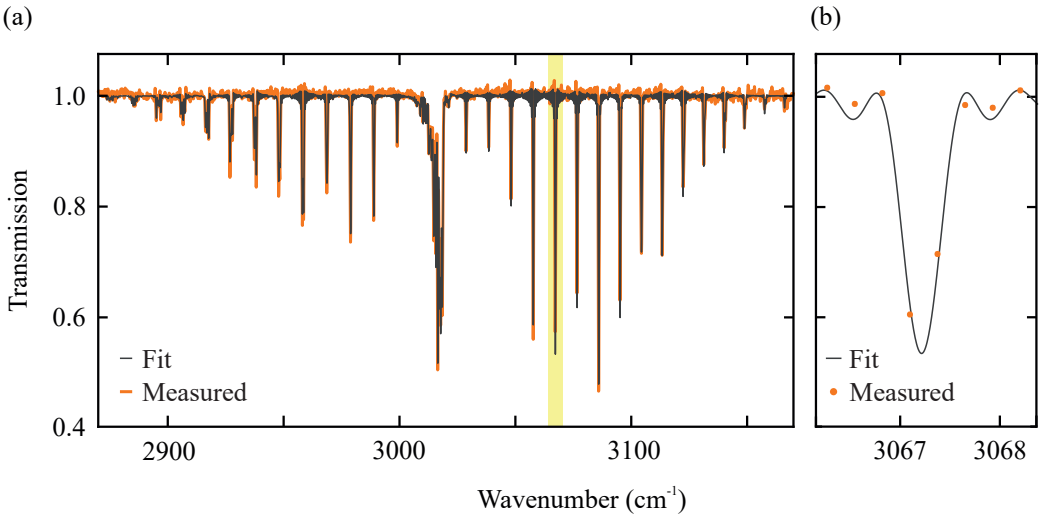

Figure 3. Measured transmission spectrum of methane, calculated from sample and reference spectrum (shown in Figure 2b) shown as orange curve/dots. A detailed view of the highlighted absorption feature is shown in part (b). The fitted model function (Eq. 1) is shown in gray.

4.2 Signal-to-noise ratio

An important limitation of the sensitivity of the spectrometer is its signal-to-noise ratio (SNR), which determines the minimum transmission change which can be distinguished from random fluctuations. The signal-to-noise ratio can be determined from the transmission spectra using a spectral range without sample absorption (in this case we use a spectral range of 2800 cm^{-1} to 2850 cm^{-1}). Without sample absorption, the transmission values are normally distributed around their expectation value of $T_0 \approx 1$. From the standard deviation σ and the mean value μ of the measured transmission we can calculate the SNR by:

$$\mathrm{SNR} = \frac{\mu}{\sigma}. \tag{3}$$

For the transmission spectrum shown in Figure 3, the signal-to-noise ratio results to 180, which corresponds to a sensitivity of 1.6 % (3σ) transmission change.

Due to the low power, photon shot noise may be an important contribution to the total noise determining the SNR. To verify this, we estimate the theoretic signal-to-noise ratio considering only photon shot noise. The noise-equivalent power of photon shot noise can be defined as:

$$P_\mathrm{N} = \sqrt{\frac{\epsilon P h\nu}{t}}\sqrt{F}, \tag{4}$$

with the detector efficiency $\epsilon = 55.8\,\%$, the SPDC power $P \approx 20\,\mathrm{nW}$, the median energy of a signal photon $h\nu = 1.24\,\mathrm{eV}$ (signal wavelength approximated to 1 µm), the single measurement time $t = 9\,\mathrm{s}$ and the excess noise factor $F \approx 5$, which describes the increase in shot noise due to the avalanche effect of the photo detector.

The available signal power in a Fourier-transform measurement with a spectral resolution of $\Delta\tilde{\nu}$ can be described by

$$S = \eta\epsilon U_{\tilde{\nu}} \Delta\tilde{\nu}, \tag{5}$$

with the interferometer efficiency $\eta \approx 0.15$ (estimated by the measured maximum interference contrast) and the power spectral density $U_{\tilde{\nu}}$, which can be approximated to a uniform distribution over a bandwidth $\tilde{\nu}_\mathrm{max} - \tilde{\nu}_\mathrm{min}$:

$$U_{\tilde{\nu}} = \frac{P}{\tilde{\nu}_\mathrm{max} - \tilde{\nu}_\mathrm{min}}. \tag{6}$$

Using equations 5,4 we can estimate a limitation to the SNR of n averaged measurements:

$$\mathrm{SNR} = \sqrt{n}\frac{S}{P_\mathrm{N}} = \eta\sqrt{\frac{\epsilon P n t}{F h\nu}}\frac{\Delta\nu}{\tilde{\nu}_\mathrm{max} - \tilde{\nu}_\mathrm{min}}. \tag{7}$$

For 100 averaged measurements with a spectral resolution of $0.56\,\mathrm{cm}^{-1}$ and a bandwidth of $725\,\mathrm{cm}^{-1}$, the SNR-limit results to ≈ 366. Taking into account the uncertainties of the above derivation, photon shot noise should be considered a significant contribution to overall noise, in contrast to classical Fourier-transform infrared spectrometers which are typically limited by detector dark noise.[18]
In the current realization, the low dark noise level of the silicon-based detector (in comparison to typical mid-infrared detectors) can not be utilized since the available SPDC power is up to six orders of magnitude lower than the output power of a black body radiator in the 3 µm to 4 µm wavelength range. In consequence, classical FTIR spectrometers as well as upconversion spectrometers achieve considerably higher signal-to-noise ratios per measurement time. Key to improving the signal-to-noise ratio of the nonlinear interferometer will be more efficient sources for correlated photons, which could be realized using other nonlinear materials, waveguides, or resonant pump enhancement.

5. CONCLUSION

Nonlinear interferometers offer new possibilities for mid-infrared spectroscopy, using correlated photon pairs far from degeneracy. We have demonstrated a nonlinear interferometer utilizing a measurement scheme and analysis in analogy to classical FTIR-spectroscopy. The interference phenomena of the correlated photon pairs allow measuring mid-infrared information with near-infrared detection.
For a performance characterization, we measured the transmission spectrum of methane around 3.3 µm wavelength. The spectrometer achieves a high spectral resolution of up to $0.56\,\mathrm{cm}^{-1}$ in a bandwidth of over $725\,\mathrm{cm}^{-1}$. The spectral resolution is only limited by the maximum delay between the interferometer arms and can be improved in future implementations. The demonstrated signal-to-noise ratio is yet significantly lower than that of classical Fourier-transform spectrometers. Photon shot noise is identified as a significant noise contribution. In the future, nonlinear interferometers may prove an alternative to established spectroscopic techniques if the available signal power can be improved.
The measurement principle can easily be extended to the infrared transparency range of lithium niobate and could be adapted to other spectral ranges, such as the fingerprint infrared range from 7 µm to 12 µm wavelength, using suitable nonlinear materials. Another interesting perspective is the application of the Fourier-transform approach to hyperspectral wide-field microscopy with correlated photons.[7]
The presented measurement approach, combining nonlinear interferometry and Fourier-transform analysis, enables the novel technique to be applied to spectroscopic tasks efficiently and precisely.

REFERENCES

[1] Zou, X. Y., Wang, L. J., and Mandel, L., "Induced coherence and indistinguishability in optical interference," *Physical review letters* **67**(3), 318–321 (1991).

[2] Burlakov, A. V., Chekhova, M. V., Klyshko, D. N., Kulik, S. P., Penin, A. N., Shih, Y. H., and Strekalov, D. V., "Interference effects in spontaneous two-photon parametric scattering from two macroscopic regions," *Physical Review A* **56**(4), 3214–3225 (1997).

[3] Chekhova, M. V. and Ou, Z. Y., "Nonlinear interferometers in quantum optics," *Advances in Optics and Photonics* **8**(1), 104 (2016).

[4] Paterova, A. V., Yang, H., An, C., Kalashnikov, D. A., and Krivitsky, L. A., "Tunable optical coherence tomography in the infrared range using visible photons," *Quantum Science and Technology* **3**(2), 025008 (2018).

[5] Vanselow, A., Kaufmann, P., Zorin, I., Heise, B., Chrzanowski, H., and Ramelow, S., "Mid-infrared frequency-domain optical coherence tomography with undetected photons," in [*Quantum Information and Measurement (QIM) V: Quantum Technologies*], *Quantum Information and Measurement (QIM) V: Quantum Technologies* , Optical Society of America (2019). T5A.86.

[6] Machado, G. J., Frascella, G., Torres, J. P., and Chekhova, M. V., "Optical coherence tomography with a nonlinear interferometer in the high parametric gain regime," *Applied Physics Letters* **117**(4), 094002 (2020).

[7] Kviatkosvky, I., Chrzanowski, H. M., Avery, E. G., Bartolomaeus, H., and Ramelow, S., "Microscopy with undetected photons in the mid-infrared," *Science Advances* **6**(42), eabd0264 (2020).

[8] Paterova, A. V., Maniam, S. M., Yang, H., Grenci, G., and Krivitsky, L. A., "Hyperspectral infrared microscopy with visible light," *Science Advances* **6**(44), eabd0460 (2020).

[9] Kutas, M., Haase, B., Bickert, P., Riexinger, F., Molter, D., and von Freymann, G., "Terahertz quantum sensing," *Science Advances* **6**(11), eaaz8065 (2020).

[10] Lemos, G. B., Borish, V., Cole, G. D., Ramelow, S., Lapkiewicz, R., and Zeilinger, A., "Quantum imaging with undetected photons," *Nature* **512**(7515), 409–412 (2014).

[11] Kalashnikov, D. A., Paterova, A. V., Kulik, S. P., and Krivitsky, L. A., "Infrared spectroscopy with visible light," *Nature Photonics* **10**(2), 98–101 (2016).

[12] Paterova, A., Lung, S., Kalashnikov, D. A., and Krivitsky, L. A., "Nonlinear infrared spectroscopy free from spectral selection," *Scientific Reports* **7**, 42608 (2017).

[13] Paterova, A., Yang, H., An, C., Kalashnikov, D., and Krivitsky, L., "Measurement of infrared optical constants with visible photons," *New Journal of Physics* **20**(4), 43015 (2018).

[14] Lindner, C., Wolf, S., Kiessling, J., and Kühnemann, F., "Fourier transform infrared spectroscopy with visible light," *Optics Express* **28**(4), 4426–4432 (2020).

[15] Wolf, S., Kiessling, J., Kunz, M., Popko, G., Buse, K., and Kühnemann, F., "Upconversion-enabled array spectrometer for the mid-infrared featuring kilohertz spectra acquisition rates," *Optics Express* **25**(13), 14504–14515 (2017).

[16] Tidemand-Lichtenberg, P., Dam, J., Andersen, H., Høgstedt, L., and Pedersen, C., "Mid-infrared upconversion spectroscopy," *Journal of the Optical Society of America B* **33**(11), D28–D35 (2016).

[17] Vanselow, A., Kaufmann, P., Chrzanowski, H. M., and Ramelow, S., "Ultra-broadband SPDC for spectrally far separated photon pairs," *Optics Letters* **44**(19), 4638 (2019).

[18] Griffiths, P. R. and de Haseth, J. A., [*Fourier transform infrared spectrometry*], Wiley-Interscience (2007).

[19] Sheahen, T., "Chirped Fourier Spectroscopy. Theory of Resolution and Contrast," *Applied Optics* **14**(4), 1004–1012 (1975).

[20] Gordon, I., Rothman, L., Hill, C., Kochanov, R., Tan, Y., Bernath, P., Birk, M., Boudon, V., Campargue, A., Chance, K., Drouin, B., Flaud, J.-M., Gamache, R., Hodges, J., Jacquemart, D., Perevalov, V., Perrin, A., Shine, K., Smith, M.-A., Tennyson, J., Toon, G., Tran, H., Tyuterev, V., Barbe, A., Császár, A., Devi, V., Furtenbacher, T., Harrison, J., Hartmann, J.-M., Jolly, A., Johnson, T., Karman, T., Kleiner, I., Kyuberis, A., Loos, J., Lyulin, O., Massie, S., Mikhailenko, S., Moazzen-Ahmadi, N., Müller, H., Naumenko, O., Nikitin, A., Polyansky, O., Rey, M., Rotger, M., Sharpe, S., Sung, K., Starikova, E., Tashkun, S., Auwera, J. V., Wagner, G., Wilzewski, J., Wcisło, P., Yu, S., and Zak, E., "The HITRAN2016 molecular spectroscopic database," *Journal of Quantitative Spectroscopy and Radiative Transfer* **203**, 3 – 69 (2017).

[21] Harvard-Smithsonian Center for Astrophysics (CFA), Cambridge, MA, USA, V.E. Zuev Insitute of Atmosperic Optics (IAO), Tomsk, Russia, and National Research Tomsk State University (TSU), Tomsk, Russia, "HITRAN on the web." hitran.iao.ru. accessed: 10.08.2020.